DOI: 10.61782/fa.2023.0887

forum acusticum 2023

EXPERIMENTAL CHARACTERIZATION OF THE IMPEDANCE OF (SUB-)MILLIMETER PERFORATIONS WITH FLOW

Simon Vandemaele[1,2*] **Hervé Denayer**[1,2] **Wim De Roeck**[1] **Wim Desmet**[1,2]
[1] Department of Mechanical Engineering, KU Leuven, Belgium
[2] Flanders Make@KU Leuven, Leuven, Belgium

ABSTRACT

For the design of more compact acoustic wall treatments for flow duct applications, (sub-)millimeter perforations can be considered as promising component for acoustic (meta)liners. By decreasing the perforation dimensions, an increased acoustic resistance and low acoustic mass reactance can be achieved, enabling the potential for wide-band absorption without jeopardizing the aerodynamic performance. The perforations' aero-acoustic properties are, however, significantly influenced by the flow conditions and configurations in which they are operating. In this paper, the flow-acoustic behavior of orifices with perforation diameters ranging from 0.5 to $3\mathrm{mm}$ is characterized using a multi-microphone three-port measurement technique. Within this framework, small perforated samples are flush-mounted in the wall of a main measurement duct, covering a side-branch measurement duct. Measurements are conducted for different grazing flow rates and the effect on the perforate resistance and external end correction is studied. Generally, the perforate resistance increases and the external end correction decreases with increasing flow rate with both effects diminishing for larger diameters at higher frequencies. Correlating the results with skin friction velocity yields an acceptable estimate for the end correction for all diameters and flow rates. For the resistance, however, no significant trend is observed.

Keywords: *acoustic impedance, (micro-)perforations, experiment, grazing flow*

**Corresponding author*: simon.vandemaele@kuleuven.be.

1. INTRODUCTION

Efficient, compact broadband sound attenuation in flow ducts is a major challenge in the design of modern day machinery. Given that the flow should be obstructed as little as possible, passive damping solutions are usually installed as wall treatments and are hence exposed to a grazing flow. Acoustic liners are one of the most popular wall treatments currently used. Conventionally, they consist of perforated duct walls, backed by a subdivided cavity which creates an array of Helmholtz resonators. Narrow-band sound absorption is achieved around the resonance frequency by a combination of viscous and flow-acoustic interaction effects occurring at the perforated surface.

Novel (meta)liner configurations build upon this conventional approach by combining different perforated materials and acoustic resonators to broaden the frequency absorption band. Decreasing orifice dimensions often plays an important role in this process. Such micro-perforations have enabled broadband absorption for room absorbers [1] due to an increased acoustic resistance and low acoustic mass reactance and have shown promising results for flow duct applications as well [2].

To describe the acoustic behavior of small orifices, the acoustic impedance is commonly used. For acoustically compact orifices in a plate with perforation ratio σ, the normalized acoustic impedance z can be defined in frequency domain as the ratio of the acoustic pressure difference over the perforates (Δp_p) to the normal surface averaged particle velocity (u_p) through the perforations:

$$z = \frac{1}{\sigma} z_p = \frac{1}{\rho_0 c_0} \frac{1}{\sigma} \frac{\Delta p_p}{u_p} = (r + i\chi) \tag{1}$$

The impedance of a single perforation is, hereby, given by z_p, the characteristic impedance of the medium under consideration is defined by $\rho_0 c_0$ (with ρ_0 the density and

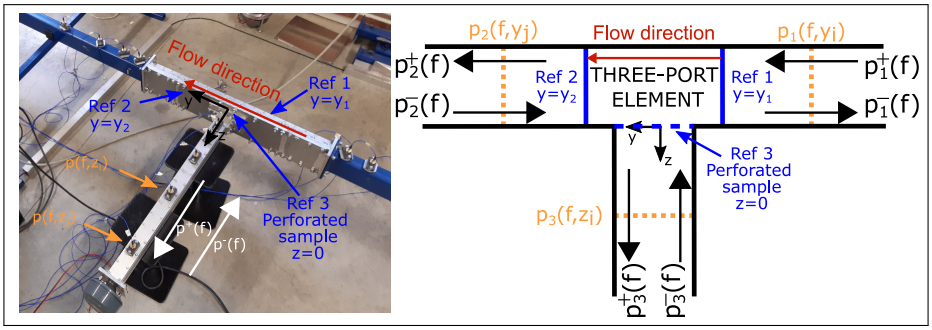

Figure 1: (Left) Detailed view of the grazing flow impedance tube mounted into the KU Leuven flow-acoustic test rig. (Right) Schematic representation of the set-up modeled as a three-port element to process for unwanted interference between flow duct and side-branch during measurement. The reference frame is indicated in blue, the used convention of complex plane wave amplitudes $p^{\pm}$ in black and the flow direction in red.

c_0 the speed of sound under ambient conditions) and the real (r) and imaginary (χ) part are referred to as the resistance and reactance, respectively. In quiescent conditions, the resistive part represents all acoustic losses caused by a.o. visco-thermal effects in and around the perforation opening. The reactive component is mostly dominated by the inertial effect of oscillating air in and around the perforations. At sufficiently small in-hole particle velocities, the acoustic impedance behaves linear [3].

For perforations operating under grazing flow with low Strouhal numbers and thick boundary layers compared to the perforation diameter, the resistance typically increases and the reactance decreases with respect to quiescent conditions. Commonly, these phenomena are attributed to an increase in acoustic losses when the acoustic waves interact with the flow shear layers over the perforations (increased resistance) and to a decrease of the oscillating fluid mass at the flow side (decreased reactance) [4]. Many observations and correlations in literature report the dependency of the grazing flow effect on mean flow parameters (e.g. the Mach number) [2, 5–7] or on inner boundary layer parameters (e.g. the friction velocity) [8–12]. The specific nature of these phenomena is, however, not yet fully understood and further experimental investigations are therefore needed. The objective of this paper is to measure the effect of grazing flow on perforations with a diameter between 0.5 and $3\mathrm{mm}$.

In the presence of grazing flow, measuring the parameters Δp_p and u_p directly, although not impossible, is very challenging. When measuring too close to the perforated surface, measured quantities will contain acoustic near field effects and aerodynamic pressure perturbations originating from the shear layer over the perforations, whereas measuring too far from the perforated surface would yield to unrepresentative impedance values. Indirect side-branch measurement techniques alleviate these issues by calculating the acoustic variables of interest based on recorded pressure or velocity values far away from the perforated surface combined with simple models. Reported configurations include a.o. one-microphone impedance tubes driven by a controlled piston source (with measured acceleration) [8, 9], variations on the two-microphone impedance tube [10] and multi-microphone impedance tubes [6, 13]. Within this paper, the latter method is adopted and extended with a (flow-)acoustic three-port description to eliminate irrelevant acoustic interference effects.

2. EXPERIMENT

2.1 Characterization of the perforation impedance

In order to evaluate Eqn. (1), both Δp_p and u_p have to be measured. An indirect measurement approach is adopted by placing a side-branch impedance tube below the perforated sample as illustrated on the left of Fig. 1 [6, 13]. When only plane waves propagate, the acoustic pressure and velocity at the bottom side of the perforations can be calculated using a limited number of pressure measurements along the impedance tube length (indicated in orange). However, acoustic interaction between the impedance tube and the flow duct could pollute the measured acoustic pressures. To eliminate these effects, the set-up is processed as a (flow-)acoustic three-port.

2.1.1 Plane wave propagation in a duct

Below the cut-off frequency of the first cross-sectional acoustic duct mode, the acoustic pressure $p(f, z_i)$ and particle velocity $u(f, z_i)$ at any arbitrary position z_i along the duct axis can be expressed as a sum of down- and upstream propagating plane waves with complex amplitudes $p^{\pm}(f, 0)$ (at a chosen reference position $z = 0$) and wavenumbers $k^{\pm}$:

$$p(f, z_i) = p^{+}(f, 0)e^{-jk^{+}z_i} + p^{-}(f, 0)e^{jk^{-}z_i} \quad (2)$$

$$u(f, z_i) = \frac{1}{\rho_0 c_0}(p^{+}(f, 0)e^{-jk^{+}z_i} - p^{-}(f, 0)e^{jk^{-}z_i}) \quad (3)$$

In the equations above, convective effects and viscothermal damping at the duct walls are accounted for in the expression of $k^{\pm}$ as corrections on the acoustic wavenumber k_0 [14]

$$k^{\pm} = k_0 \frac{\theta(f)}{1 \pm \theta(f)M} \quad (4)$$

with M representing the free stream surface averaged Mach number and $\theta(f)$ the complex, frequency dependent, Kirchhoff coefficient as expressed in [6].

If the pressure spectra at two different positions $p(f, z_i)$ are known, a system of Eqn. (2) can be be solved for the unknown pressure wave amplitudes $p^{\pm}(f, 0)$. For frequencies where the microphone distance coincides with a multiple of half a wavelength, this set of equations becomes undetermined. Older measurement techniques resolved this issue by adapting the microphone distance for every frequency (see e.g. [10]). In the present work a multi-microphone approach is used in order to obtain an overdetermined set of Eqns. (2), which is solved with a least-squares approach [15].

2.1.2 Three-port characterization of the measurement set-up

Acoustic interference effects in the different branches of the flow duct network can influence the pressure measurements in the impedance tube. This is especially the case when the flow duct terminations are not anechoic and hence reflect acoustic waves towards the measurement section. To take into account this unwanted interference, the perforated section is characterized as a (flow-)acoustic three-port element, as illustrated on the right of Fig. 1. This model relates the in- and outgoing acoustic plane wave amplitudes $p^{\pm}$ using a linear matrix relation with frequency dependent coefficients:

$$\begin{Bmatrix} p_1^{-}(f) \\ p_2^{+}(f) \\ p_3^{+}(f) \end{Bmatrix} = \begin{bmatrix} R_{11} & T_{21} & T_{31} \\ T_{12} & R_{22} & T_{32} \\ T_{13} & T_{23} & R_{33} \end{bmatrix} \begin{Bmatrix} p_1^{+}(f) \\ p_2^{-}(f) \\ p_3^{-}(f) \end{Bmatrix} \quad (5)$$

This representation is called the scattering matrix and its coefficients represent transmission T and reflection R coefficients of the element when the terminations are anechoic. As such, this formulation is independent of the up- and downstream boundary conditions and excludes possible acoustic interference effects from the final results.

In the convention used in this paper, the upstream flow duct is denoted with the subscript '1', the downstream flow duct as '2' and the impedance tube as '3'. The plane wave amplitudes can be obtained from a plane wave decomposition based on pressure measurements at different locations in each duct as described in section 2.1.1.

From matrix Eqn. (5), it is clear that three independent sets of amplitudes $p^{\pm}$ must be known to solve for the 9 unknown coefficients. These are obtained using the multiple source method [16].

2.1.3 Calculation of the perforation impedance

In the impedance expression Eqn. (1), Δp_p denotes the acoustic pressure difference over the perforation. In the current set-up, looking from the perspective of an excitation in the side-branch (duct 3), the dynamic pressure at the side-branch side is equal to $p_3(f, 0)$ whereas the dynamic pressure at the flow side can be estimated by the average of $p_1(f, y_1)$ and $p_2(f, y_2)$ when the distance between y_1 and y_2 is small compared to the considered acoustic wavelength. This dynamic pressure accounts for the acoustic radiation of the perforates in the enclosed grazing medium. Ingard and Singal [17] postulated that, for low mean velocities ($M < 0.2$), the radiation impedance can be considered to be independent of the flow velocity. The effect of grazing flow on the acoustic impedance can hence be studied by only investigating the one-sided impedance as seen from duct 3, without accounting for the pressure at the flow duct side.

The averaged acoustic particle velocity at the perforation opening u_p is determined by $1/\sigma$ times the acoustic velocity in the side-branch $u_3(f, 0)$. In terms of the pressure wave amplitudes $p_i^{\pm}(f, 0)$, and following the convention, introduced in Fig. 1, the impedance expression can then be written as

$$z = -\frac{p_3^{+}(f, 0) + p_3^{-}(f, 0)}{p_3^{+}(f, 0) - p_3^{-}(f, 0)} \quad (6)$$

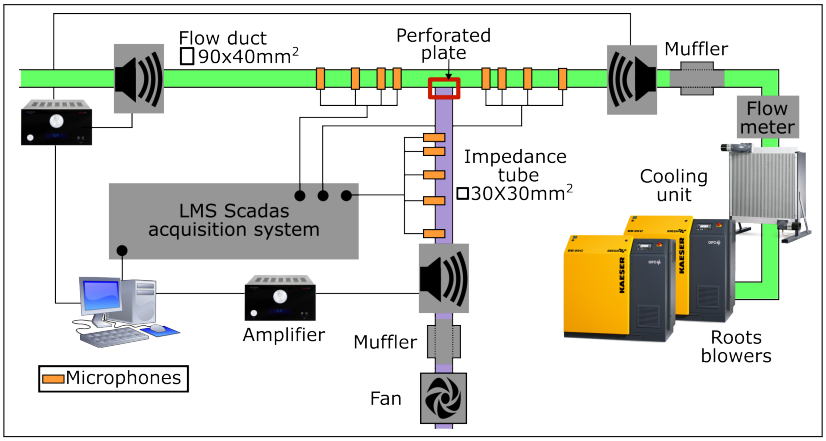

Figure 2: Experimental set-up: perforated samples (red) are mounted in the side wall of a flow duct (green) covering a side-branch measurement duct (purple).

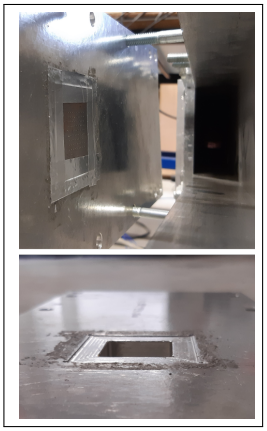

Figure 3: Flush mounted sample in the flow duct.

which can be reformulated in terms of the scattering matrix reflection coefficient R_{33} of Eqn. (5) as

$$z = \frac{1 + R_{33}(f)}{1 - R_{33}(f)} \tag{7}$$

2.2 Measurement set-up

Figure 2 schematically depicts the experimental set-up consisting of a main rectangular flow duct (90mm by 40mm, green), the square side-branch measurement duct (30mm by 30mm, purple) and the perforated sample mounted in the junction of both components (red square). A fully developed turbulent flow, with a free stream surface averaged Mach number (M) between 0 and 0.09, is supplied to the perforated section through the main flow duct by two frequency regulated roots blowers. A cooling unit ensures stable measurement conditions, a built-in vortex flowmeter monitors both temperature and flow rate and a muffler damps out any unwanted noise coming from the upstream flow source. Specific care is taken to create a purely grazing flow on top of the investigated orifices. The impedance tube side-branch is, therefore, equipped with a fan to counteract any pressure difference over the mounted sample to avoid bias flow through the perforations.

All measurement ducts are equipped with an amplifier-fed loudspeaker and flush-mounted PCB 378C10 microphones (4 in the up-/downstream duct, 5 in the impedance tube), both connected to an LMS Scadas acquisition system (controlled by Test.Lab v17 software). To limit unwanted near field effects in the recorded pressure signals, the first microphone in each duct is placed sufficiently far from the perforated section. The position of the other microphones is selected to have a well conditioned plane wave decomposition for all considered frequencies.

Perforations with a diameter (d) of 0.5, 1 ,2 and 3mm are drilled in a 0.5mm thick steel plate (50mm by 50mm) with either electrical discharge machining (for the smallest diameter) or mechanical drilling. An equidistant square perforation pattern is selected with a centerline-to-centerline distance equal to five diameters, following the theoretical limit of Melling at which interaction effects between the perforations should be negligible [18]. Table 1 gives an overview of the samples' porosity.

Table 1: Orifice dimensions

Diameter (d)	% open area (σ)	Thickness (t)
0.5mm	1,77%	0.5mm
1mm	2.18%	0.5mm
2mm	3.14%	0.5mm
3mm	3.14%	0.5mm

Figure 3 shows the perforated samples flush mounted at the side of the flow duct by placing them in a cavity with double-sided tape. Furthermore, all plate edges at the flow side are sealed with aluminum tape to limit the flow disturbance. To assess the repeatability of the mounting strategy, the $d = 0.5\text{mm}$ plate was remounted and mea-

sured four times both in the absence and presence of grazing flow ($M = 0.05$). All impedance measurements were in good agreement, as illustrated with the 95% confidence interval (shaded black and orange) in Figs. 4a and b.

2.3 Measurement procedure

In order to stay within the plane wave limits of the flow duct cross-section, the frequency range of interest is selected from 150Hz to 1850Hz. The pressure fluctuations $p(f, z_i)$ are not measured directly, but are replaced with the transfer functions between the recorded pressures and the loudspeaker signal, allowing to discard uncorrelated contributions to the pressure signals, which would lead to an accumulation of measurement errors. A stepped sine excitation signal in steps of 50Hz with 20 spectral averages is used to measure in turbulent flow conditions. The excitation level is set as large as possible, while keeping the acoustic particle velocity in the perforation openings within the linear acoustic behavior limits. Using, respectively, 4 and 5 microphones in the flow ducts and side-branch, a suppression of measurement errors is achieved when solving the overdetermined set of Eqns. (2). Furthermore, the availability of multiple microphones allows the use of the iterative plane wave decomposition procedure of reference [19] which solves the set of equations for additional environmental parameters (c_0, M ...), effectively reducing uncertainties on the measured pressure plane wave amplitudes.

3. DISCUSSION OF THE RESULTS

The effect of grazing flow on the normalized acoustic impedance of a single perforation ($z_p = \sigma z$) with varying diameter is summarized in Fig. 4. Measurements are performed for four different diameters (0.5mm (+), 1mm (○), 2mm (□) and 3mm (▽)), both without flow (black) and for five different Mach numbers (0.05 (orange), 0.06 (red), 0.07 (blue), 0.08 (green) and 0.09 (purple)).

The measured perforate resistance (σR) is depicted in the left column. In the absence of flow, the resistance slightly increases with frequency for all perforation diameters. For the smallest diameter (Fig. 4a), the grazing flow significantly increases the resistance over the entire frequency range and the observed increase seems to be more or less frequency independent and proportional with M [2, 6]. When the perforations become larger (e.g. $d = 2$mm (Fig. 4c)), the flow effects are still significant in the lower frequency range, but become smaller as the frequency increases which is also observed by Lee and Ih for perforations with a diameter varying between 3 and 8mm [20]. At the smallest flow rates, the resistance drops below the no flow values as also reported in [10]. Despite this frequency dependency, the resistance increment shows a similar behavior for all grazing flow rates, especially at the lower frequencies.

Looking into the effect of varying diameters for the same flow rate in more detail (Fig. 4e), two distinct frequency ranges can be observed. At the lower frequencies, increasing the perforation diameter increases the resistance, whereas it decreases at higher frequencies, previously reported by Lee and Ih [20]. The frequency at which the trend reverses is higher for higher flow rates.

To study the grazing flow effect on the inertial part of the impedance, the exterior end correction δ_e is calculated from the measured reactance χ:

$$\delta_e = \frac{\sigma\chi}{k} - \frac{j2\pi f}{c} t \left(1 - \frac{2}{\kappa\sqrt{(-j)}} \frac{J_1(\kappa\sqrt{-j})}{J_0(\kappa\sqrt{-j})} \right)^{-1} \quad (8)$$

The latter term represents the theoretical, internal acoustic impedance for a narrow perforation of limited thickness [5] in which J_0 and J_1 represent the zero and first order Bessel functions of the first kind and κ is given by

$$\kappa = \frac{d}{2}\sqrt{\frac{\pi f}{2\nu}} \quad (9)$$

with ν the kinematic viscosity of air.

In the absence of flow, δ_e behaves more or less frequency independent up to 1000Hz and starts to slightly increase at higher frequencies. For $d = 0.5$mm, the constant value at lower frequencies is in reasonable agreement with the end correction term ($0.85d(1 - 0.7\sqrt{\sigma})$), indicated with the grey dashed line) used by Guess [5], while a lower end correction is measured for $d = 2$mm (Figs. 4b and 4d). When the perforation diameter increases for the same plate thickness, the end correction, representing the exterior inertial effects, logically increases as well.

In general, the grazing flow effectively reduces the exterior end correction for all considered perforation diameters. Similar as for the resistance, the decrement behaves more or less frequency-independent for $d = 0.5$mm resulting in a shift of the curves, proportional with Mach number (Fig. 4b). However, for $d = 2$mm, the end correction decreases with frequency in the low frequency range, reaches a minimum and starts to increase again towards the no flow end correction at higher frequencies (Fig. 4d). This increase starts at lower frequencies for larger diameters (Fig. 4f).

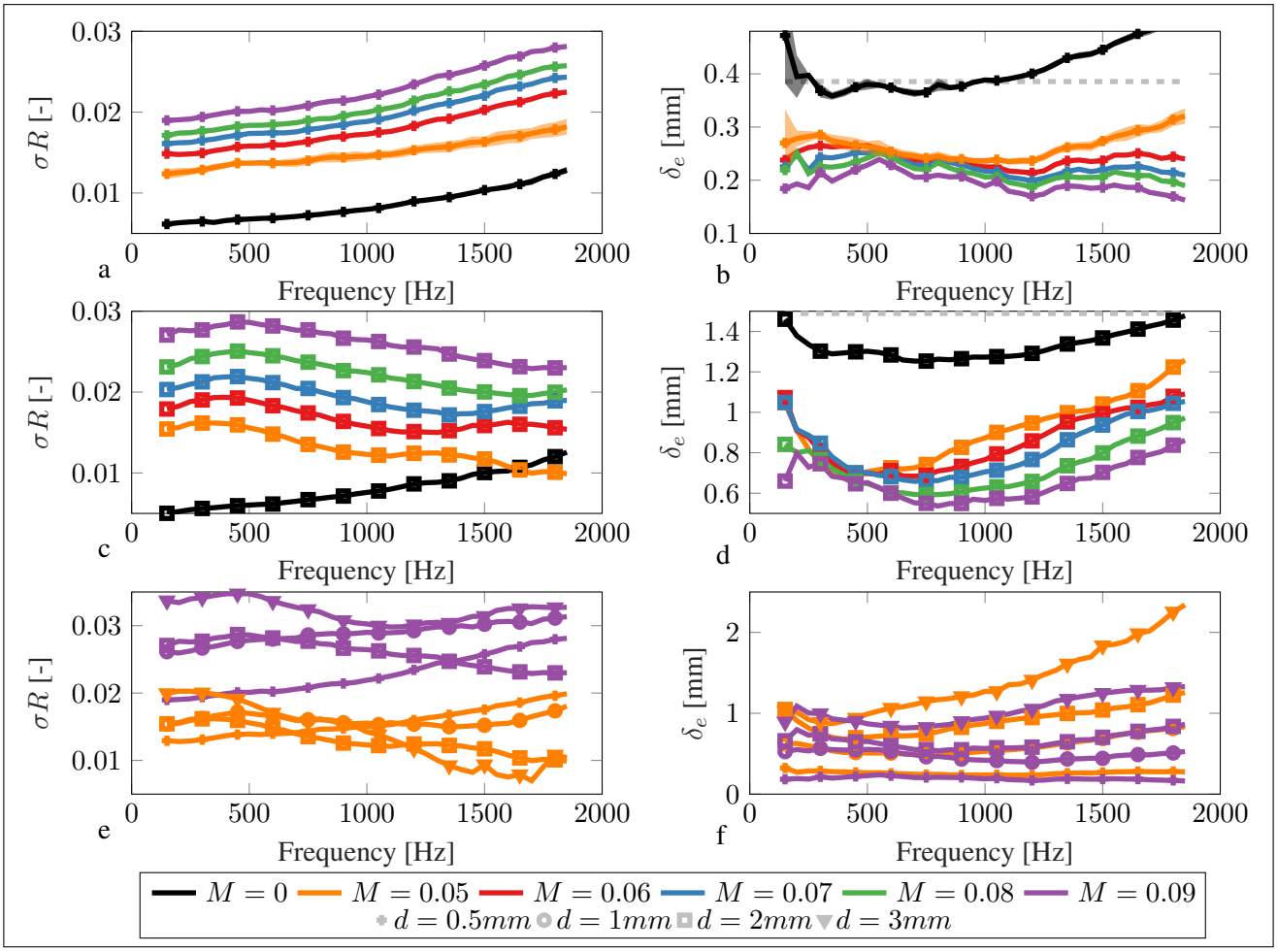

Figure 4: Measured perforate resistance (σR) and external end correction (δ_e): (a,b) effect of M for $d = 0.5mm$, (c,d) effect of M for $d = 2mm$ and (e,f) effect of d for $M = 0.05$ and $M = 0.09$

Based on these findings, it is clear that the trends observed in Fig. 4 show a clear dependency on both flow rate and perforation diameter. To further investigate the observed difference in grazing flow effect, the measured data can be plotted versus the Strouhal number ($St = 2\pi f d/u*$) based on the skin friction velocity $u*$ (see a.o. references [8, 9]). This non-dimensional variable relates the acoustic frequency (f) to the frequency of turbulent eddies with size d that are convected over the orifice.

By definition, $u*$ is determined by the wall shear stress τ_w:

$$u* = \sqrt{\frac{\tau_w}{\rho}} \tag{10}$$

which for the here considered, fully developed, turbulent flows can be estimated based on the averaged flow velocity U and the Darcy friction coefficient f_D calculated using the Blasius equation [21]:

$$\tau_w = \rho U \frac{f_D}{8}, f_D = \frac{0.184}{Re^{0.2}} \tag{11}$$

The Reynolds number Re is based on the hydraulic diameter of the rectangular duct.

Figure 5 shows the perforation resistance (scaled with $\rho u*$) and exterior end correction (scaled with the no flow exterior end correction $\delta_{e,NF}$ as a function of St. The x-axis is plotted in logarithmic scale for the sake of clarity. For each diameter, the resistance for different Mach num-

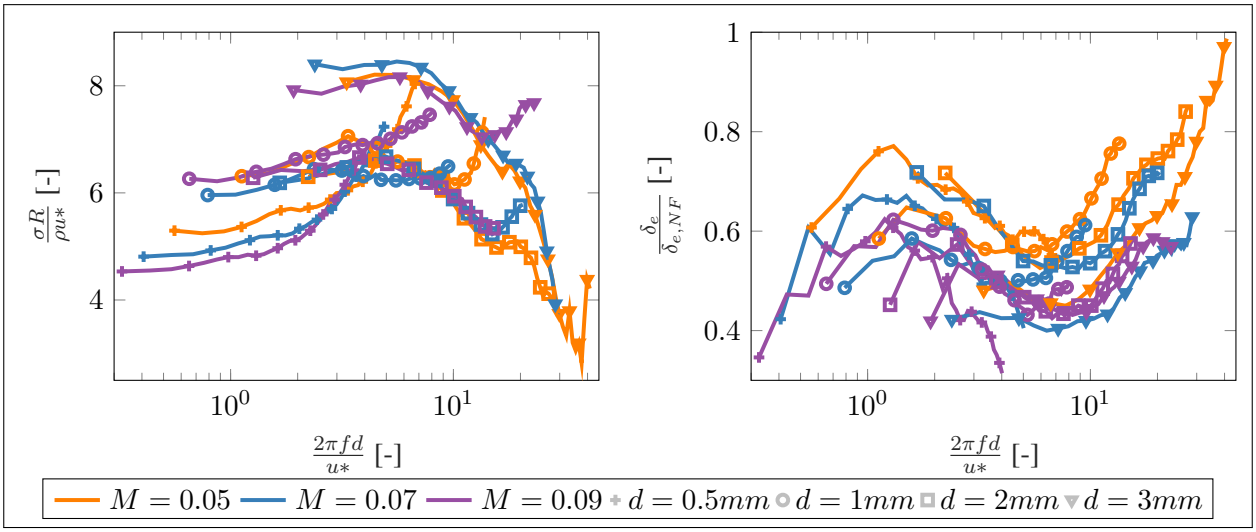

Figure 5: Nondimensionalized perforate resistance (σR) and external end correction (δ_e) plotted against skin friction velocity based Strouhal number.

bers starts to collapse at higher St; indicating a potential linear relationship with $u*$. In the lower St range, scaling with another flow parameter might, however, be more appropriate, indicated by the larger deviation in the results for $d = 0.5mm$. For the two smallest diameters, the resistance seems to behave similarly and the same is observed for the two largest diameters. The currently used parameters, however, seem to be insufficient to draw well-defined conclusions.

Better agreement is obtained for the trend in end correction where the results for different Mach numbers and orifice diameters start to collapse. Above $St = 1$, the end correction decreases to a minimum around $St \approx 6$. This value is approximately identical for all measurements. At higher St the end correction increases towards the no flow value. At this point, the acoustic field starts to dominate the orifice behavior over the aerodynamic field. Goldman and Chung [9] reported this phenomenon to happen around $St = 40$ which is in agreement with the current results. At $St < 1$, an initial increase with St is detected. This range corresponds to measurement conditions (low f, small d, high M) which are most challenging and requires some further investigations.

4. CONCLUDING REMARKS

This paper measures the grazing flow effect on the acoustic resistance and exterior end correction of orifices with perforation diameter in the $0.5 - 3\mathrm{mm}$ range. Within this framework, the perforated samples are flush-mounted in a flow duct, covering a side-branch measurement duct, and are subjected by different grazing flow velocities with a free stream averaged Mach number between 0 and 0.09. To account for unwanted acoustic interactions between the different ducts, a three-port measurement technique is adopted.

Increasing the grazing flow increases the resistance and decreases the exterior end correction at the lower frequencies for all diameters. For small diameters, the flow contribution on the resistance is independent of frequency, whereas, a decreasing flow resistance with increasing frequency is observed for larger diameters. A similar trend can also be noticed in the end correction with flow where a constant reduction occurs for all frequencies for small diameters and a diminishing trend is observed for larger perforations at higher frequencies.

Plotting the measured end corrections with respect to the skin friction based Strouhal number yields a single trend for all diameters and flow rates. For the resistance values, good agreement is only obtained for each diameter separately.

5. ACKNOWLEDGMENTS

Internal Funds KU Leuven are gratefully acknowledged for their support.

6. REFERENCES

[1] D.-Y. Maa, "Microperforated panel wide-band absorber," *Noise Control Engineering Journal*, vol. 29, pp. 77–84, 1987.

[2] S. Allam and M. Åbom, "A new type of muffler based on microperforated tubes," *Journal of Vibration and Acoustics*, vol. 133, pp. 031005 1–8, Mar. 2011.

[3] U. Ingard and H. Ising, "Acoustic nonlinearity of an orifice," *The Journal of the Acoustical Society of America*, vol. 42, pp. 6–17, July 1967.

[4] D. Ronneberger, "The acoustical impedance of holes in the wall of flow ducts," *Journal of Sound and Vibration*, vol. 24, pp. 133–150, Sept. 1972.

[5] A. Guess, "Calculation of perforated plate liner parameters from specified acoustic resistance and reactance," *Journal of Sound and Vibration*, vol. 40, no. 1, pp. 119–137, 1975.

[6] S. Vandemaele, H. Denayer, W. De Roeck, and W. Desmet, "Experimental characterization of the acoustic behavior of micro-perforations under grazing flow," in *Proc. of the AIAA Aviation 2021 forum*, p. 2268, 2021.

[7] K. N. Rao and M. Munjal, "Experimental evaluation of impedance of perforates with grazing flow," *Journal of Sound and Vibration*, vol. 108, no. 2, pp. 283–295, 1986.

[8] A. Goldman and R. L. Panton, "Measurement of the acoustic impedance of an orifice under a turbulent boundary layer," *The Journal of the Acoustical Society of America*, vol. 60, no. 6, pp. 1397–1405, 1976.

[9] A. Goldman and C. Chung, "Impedance of an orifice under a turbulent boundary layer with pressure gradient," *The Journal of the Acoustical Society of America*, vol. 71, no. 3, pp. 573–579, 1982.

[10] N. Dickey, A. Selamet, and M. Ciray, "An experimental study of the impedance of perforated plates with grazing flow," *The Journal of the Acoustical Society of America*, vol. 110, no. 5, pp. 2360–2370, 2001.

[11] J. Kooi and S. Sarin, "An experimental study of the acoustic impedance of helmholtz resonator arrays under a turbulent boundary layer," in *Proc. of the 7th AIAA Aeroacoustics Conference*, pp. AIAA–81–1998, 1981.

[12] R. Kirby and A. Cummings, "The impedance of perforated plates subjected to grazing gas flow and backed by porous media," *Journal of sound and vibration*, vol. 217, no. 4, pp. 619–636, 1998.

[13] G. Kooijman, A. Hirschberg, and J. Golliard, "Acoustical response of orifices under grazing flow: Effect of boundary layer profile and edge geometry," *Journal of Sound and Vibration*, vol. 315, pp. 849–874, Sept. 2008.

[14] E. Dokumaci, "A note on transmission of sound in a wide pipe with mean flow and viscothermal attenuation," *Journal of Sound and Vibration*, vol. 208, pp. 653–655, Dec. 1997.

[15] T. Fujimori, S. Sato, and H. Miura, "An automated measurement system of complex sound pressure reflection coefficients," in *Proc. of Inter-Noise and Noise-Con*, vol. 1984, pp. 1009–1014, Institute of Noise Control Engineering, 1984.

[16] M. Munjal and A. Doige, "Theory of a two source-location method for direct experimental evaluation of the four-pole parameters of an aeroacoustic element," *Journal of Sound and Vibration*, vol. 141, no. 2, pp. 323–333, 1990.

[17] U. Ingard and V. K. Singhal, "Upstream and downstream sound radiation into a moving fluid," *The Journal of the Acoustical Society of America*, vol. 54, no. 5, pp. 1343–1346, 1973.

[18] T. H. Melling, "The acoustic impendance of perforates at medium and high sound pressure levels," *Journal of Sound and Vibration*, vol. 29, pp. 1–65, July 1973.

[19] H. Denayer, W. De Roeck, and W. Desmet, "Experimental validation of the two-port impedance eduction method," in *Proc. of the 25th AIAA/CEAS Aeroacoustics Conference*, p. 2515, 2019.

[20] S.-H. Lee and J.-G. Ih, "Empirical model of the acoustic impedance of a circular orifice in grazing mean flow," *The Journal of the Acoustical Society of America*, vol. 114, no. 1, pp. 98–113, 2003.

[21] X. Fang, Y. Xu, and Z. Zhou, "New correlations of single-phase friction factor for turbulent pipe flow and evaluation of existing single-phase friction factor correlations," *Nuclear Engineering and Design*, vol. 241, no. 3, pp. 897–902, 2011.